

Normal incidence InAs/Al_xGa_{1-x}As quantum dot infrared photodetectors with undoped active region

Zhonghui Chen,^{a)} O. Baklenov, E. T. Kim, I. Mukhametzhanov, J. Tie, and A. Madhukar
Departments of Materials Science and Physics, University of Southern California, Los Angeles, California 90089-0241

Z. Ye and J. C. Campbell
Microelectronics Research Center, Department of Electrical Engineering, The University of Texas at Austin, Austin, Texas 78712

(Received 21 November 2000; accepted for publication 24 January 2001)

We have performed a comprehensive investigation of *n*-type quantum dot infrared photodetectors (QDIPs) based on InAs/GaAs epitaxial island quantum dots (QDs) grown via the innovative punctuated island growth technique. The structural properties of the QDs were investigated with cross-sectional transmission electron microscopy and atomic force microscopy. The electronic properties of the QDs inserted in QDIP devices were investigated with photoluminescence (PL), PL excitation, and intra- and inter-band photocurrent spectroscopy. The influence of AlGaAs layers inserted into the QDIP active regions on the performance of dark current and inter- and intra-band photocurrent was examined. Initial results on intra-band responsivity and detectivity of these QDIPs at 77 K with undoped active region show promise for application. © 2001 American Institute of Physics. [DOI: 10.1063/1.1356430]

INTRODUCTION

Self-assembled semiconductor quantum dots (QDs) are particularly attractive candidates for middle and long wavelength (3–14 μm) infrared (IR) photodetectors due to their intrinsic sensitivity to normally incident infrared light, the longer lifetime of excited electrons due to greatly suppressed electron-phonon scattering,^{1,2} and potentially significantly lower dark current.³ The reported results on middle- and long-wavelength InAs/GaAs and InGaAs/GaAs quantum dot infrared photodetectors (QDIPs) show promise.^{4–10} The QDIPs in these previous studies all had doped active regions. We have studied *n*-type InAs QDIPs with both undoped and doped active InAs multiple QD regions. Our experimental results indicate that InAs/GaAs QDIPs with an undoped active region show smaller dark current than those with a doped active region. In this article, we mainly focus on the InAs/AlGaAs QDIP structures with undoped active region. The electrons in the active InAs QDs are contributed from highly doped contact layers. The QDIPs reported here are based on GaAs-capped InAs QDs grown via an innovative technique, called punctuated island growth (PIG),¹¹ which significantly narrows the photoluminescence (PL) linewidth of the inhomogeneous QD distribution down to ~25 meV (~35 meV) in the case of single (five) QD layer samples.

EXPERIMENTAL PROCEDURES

The QDIP samples were grown on GaAs(001)±0.1° substrates via solid-source molecular beam epitaxy (MBE). The InAs QDs were deposited at 500 °C at a growth rate of 0.22 ML/s under As pressure of 7×10⁻⁶ Torr. GaAs cap

layers were grown at 350 °C via migration enhanced epitaxy (MEE) to minimize intermixing between InAs and GaAs. This approach also enhances PL efficiency as compared with the usual MBE capping approach at the same growth condition.¹² An undoped active InAs QD region was inserted between highly Si-doped top and bottom GaAs contact layers and comprises a stack of five 3.0 ML InAs QDs grown via the PIG approach utilizing the deposition sequence (2 ML InAs+60 s punctuation+1 ML InAs). Note that, in the PIG approach, growth punctuation is first done in the well-formed island regime and then additional material is deposited to allow smaller islands to catch up with larger, base-width-self-limited, islands.¹¹ This allows formation of larger and more uniform sized islands without much additional island formation, thus giving rise to PL linewidths as narrow as 18 meV.¹³ The spacer between the bottom (top) contact layer and the nearest QD layer had a thickness of 220 (240) ML. The spacers between the active QDs have a thickness of 150 ML. In this article, we present studies of QDIPs with two kinds of spacer structures. In one type of structure, referred to as S-GaAs, the spacer material is GaAs. In the other type of structure, referred to as S-AlGaAs, 21 ML AlAs/GaAs (1 ML/2 ML) short-period superlattices (SPSLs) are inserted to replace 21 ML of GaAs on both sides of each QD layer. The lower AlAs/GaAs SPSLs are located at a distance of 2 ML below the QD layer, while the upper SPSLs are deposited after growth of a 30 ML GaAs capping layer above the QD layer. The AlAs/GaAs SPSLs are grown at 500 °C via MEE approach. The 30 ML capping GaAs is also grown via MEE but at 350 °C. The undoped epitaxial GaAs layer is *p* type with a background doping level of <5×10¹⁴/cm³.

Standard photolithography and wet chemical etching procedures were used for QDIP sample processing. The me-

^{a)}Electronic mail: zhonghui@usc.edu

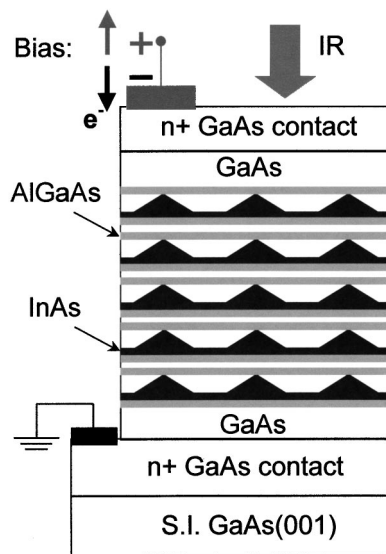


FIG. 1. Schematic of QDIP test structures (e.g., S-AlGaAs).

samples have a diameter of $250 \mu\text{m}$ with alloyed AuGe/Ni/Au contacts. Inter- and intra-band photocurrent spectroscopy was performed with a Fourier transform infrared (FTIR) spectrometer integrated with a cryostat and a current preamplifier. Spectral intra-band responsivity was measured with a monochromatic spectrometer equipped with a global source and a calibrated HgCdTe IR photodetector. All photocurrent data were measured in the normal incidence configuration. The bias polarity is relative to the grounded bottom contact. A schematic of the test QDIP structures is shown in Fig. 1. The noise characteristics were measured with both a HP noise-figure meter and a lock-in preamplifier. The photocurrent spectra were calibrated with a pyroelectric detector.

RESULTS AND DISCUSSION

Figure 2 shows contact-mode ambient atomic force microscopy (AFM) data (measured with the same tip) on uncapped 3 ML PIG InAs QD samples serving as counterparts for S-GaAs and S-AlGaAs QDIP samples. The average QD height ($59 \pm 17 \text{ \AA}$) of the S-AlGaAs counterpart is slightly smaller than that of the S-GaAs counterpart ($74 \pm 16 \text{ \AA}$). The QD density ($625 \pm 41/\mu\text{m}^2$) of the S-AlGaAs counterpart is similar to that ($673 \pm 60/\mu\text{m}^2$) of the S-GaAs counterpart. The average “QD width” corresponding to full width at half maximum (FWHM) of the AFM scan profile is $261 \pm 42 \text{ \AA}$ for the S-AlGaAs counterpart, which is slightly larger than $253 \pm 25 \text{ \AA}$ for the S-GaAs counterpart. Volumetric analysis of AFM data (based on a cone-shape assumption) along with cross-sectional transmission electron microscope (XTEM) images on the S-GaAs counterpart indicate these 3 ML InAs QDs have a base length of $\sim 210 \text{ \AA}$ and a slope of $\sim 36^\circ$.¹³ Figures 3(a) and 3(b) show XTEM images of S-GaAs and S-AlGaAs, respectively. Both indicate the existence of five-layer InAs QDs as well as wetting layers. Note that, for S-GaAs [in Fig. 3(a)], the QD density in the top layer is smaller than in the lower layers, while the QD density in S-AlGaAs is similar for all layers. Figure 3(b) also shows clear contrast between AlGaAs and GaAs layers. The mac-

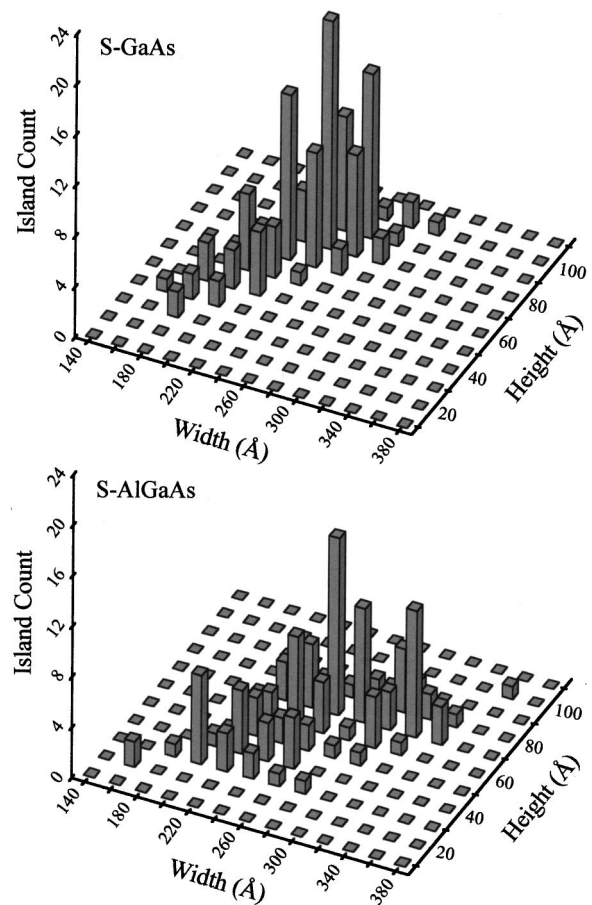


FIG. 2. AFM-determined island size distribution for the counterpart samples of S-GaAs (upper panel) and S-AlGaAs (lower panel).

roscopic defect density in these QDIPs was estimated to be $\sim 10^8 \text{ cm}^{-2}$ ($\sim 10^7 \text{ cm}^{-2}$) for S-GaAs (S-AlGaAs) based on the X-TEM measurements.

PL spectra (Fig. 4) of the QDIP samples at 78 K show a main peak at 1.060 eV (S-GaAs) and 1.066 eV for (S-AlGaAs) and a small broad shoulder on the higher energy side. The main PL peak corresponds to the QD ground state transitions. The small broad PL shoulder is most probably due to smaller QDs. The FWHM of the main peak is 36 meV (25 meV) for S-GaAs (S-AlGaAs). The narrow PL linewidth enables us to get more information on the QD electronic structure. Systematic high-density PL and PL excitation (PLE) studies were performed on this class of QDs, and the electronic structures were identified.¹³ PLE studies were also performed on the QDIP structures. Figure 5 shows PLE spectra of S-GaAs and S-AlGaAs at 78 K. The PLE spectrum recorded with a detection energy at the PL peak 1.060 eV (1.066 eV) clearly reveals five peaks at 1.092, 1.120, 1.143, 1.188, and 1.227 eV (1.099, 1.131, 1.155, 1.205, and 1.261 eV) for S-GaAs (S-AlGaAs). The PLE peak at 1.090 eV (1.099 eV) differs from detection energy by 32 meV (33 meV) which is close to the QD longitudinal-optical (LO) phonon energy, and thus corresponds to LO phonon replica.¹⁴ The other PLE peaks can be attributed to QD excited states at 60, 83, 128, and 167 meV (65, 89, 139, and 195 meV) above the ground transition for S-GaAs

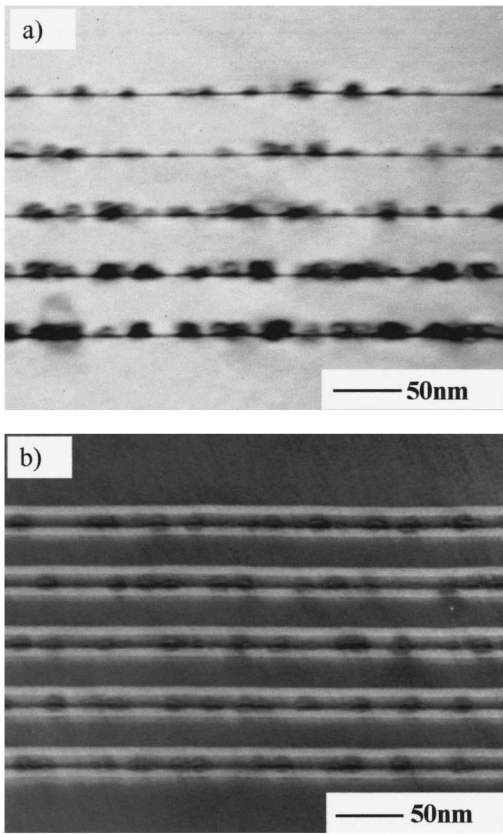


FIG. 3. Cross-sectional TEM images of S-GaAs (a) and S-AlGaAs (b).

(S-AlGaAs). The PLE peaks of S-AlGaAs blueshift relative to the corresponding peaks of S-GaAs.

Inter-band transitions in these QDs placed in an *n-i-n* QDIP configuration were also detected using FTIR photocurrent spectroscopy, indicating that the electron level occupancy was less than two per QD. Figure 6 shows a typical inter-band FTIR photocurrent spectra on S-GaAs (bias: +0.33 V) and S-AlGaAs (bias: +0.40 V) at room temperature. Multiple peaks at 0.996, 1.08, 1.16, and 1.23 eV (1.01, 1.10, 1.15, 1.20, and 1.27 eV) are clearly resolved for S-GaAs and S-AlGaAs. Compared with the PL/PLE results described above, the peaks with the lowest energy at 0.996

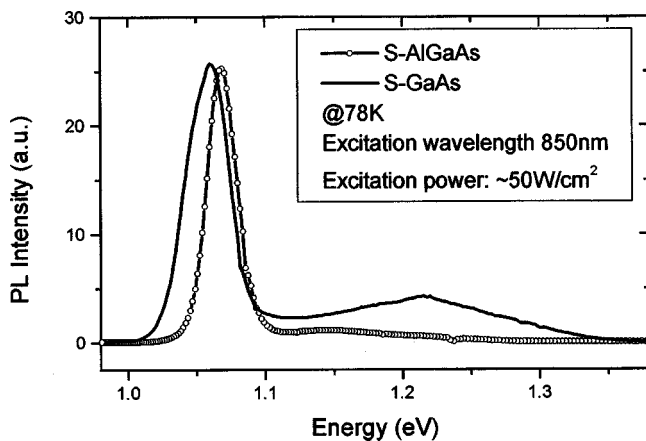


FIG. 4. PL spectra of S-GaAs and S-AlGaAs at 78 K.

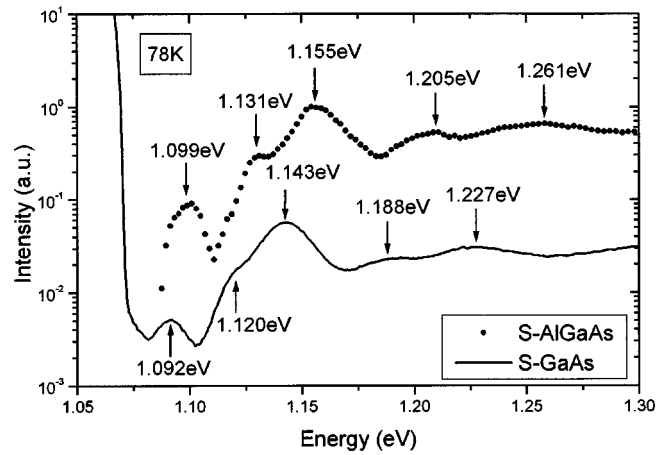


FIG. 5. PLE spectra of S-GaAs and S-AlGaAs at 78 K at a detection energy of 1.060 and 1.066 eV, respectively.

and 1.01 eV can be attributed to the ground state transitions of QDs in the S-GaAs and S-AlGaAs, respectively. The rest of the peaks can be attributed to excited states with excitation energy of 84, 164, and 234 meV (92, 140, 192, and 264 meV) relative to the ground state for S-GaAs (S-AlGaAs). These observed excited states, except that at 234 meV (264 meV), are consistent with those observed in the PLE spectrum. The observation of the additional higher excited states at 234 meV (264 meV) reflects the fact that the near infrared inter-band photocurrent spectroscopy is more sensitive to high excited states than PLE spectroscopy. Although detailed transport mechanisms of inter-band photocurrent in QDIPs with *n-i-n* configuration are not very clear so far, photocurrent serves as a very useful probe for QDIPs. The inter-band photocurrent spectroscopy is a complementary method to PLE and to intra-band photocurrent spectroscopy described below.

We next present *intra-band* photocurrent spectroscopy findings that offer more direct information on the QD electron states. Figures 7(a) and 7(b) show typical middle infrared FTIR photocurrent spectra for S-GaAs (at a bias of +0.4 V) and S-AlGaAs (at a bias of -1.00 V), respectively, at 40, 77, and 100 K. The peak position of the photocurrent spectra

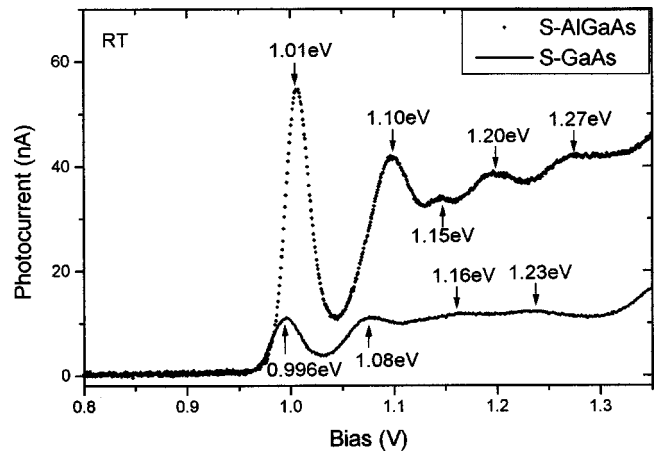


FIG. 6. Room temperature near infrared inter-band photocurrent spectra of S-GaAs and S-AlGaAs (*n-i-n* configuration).

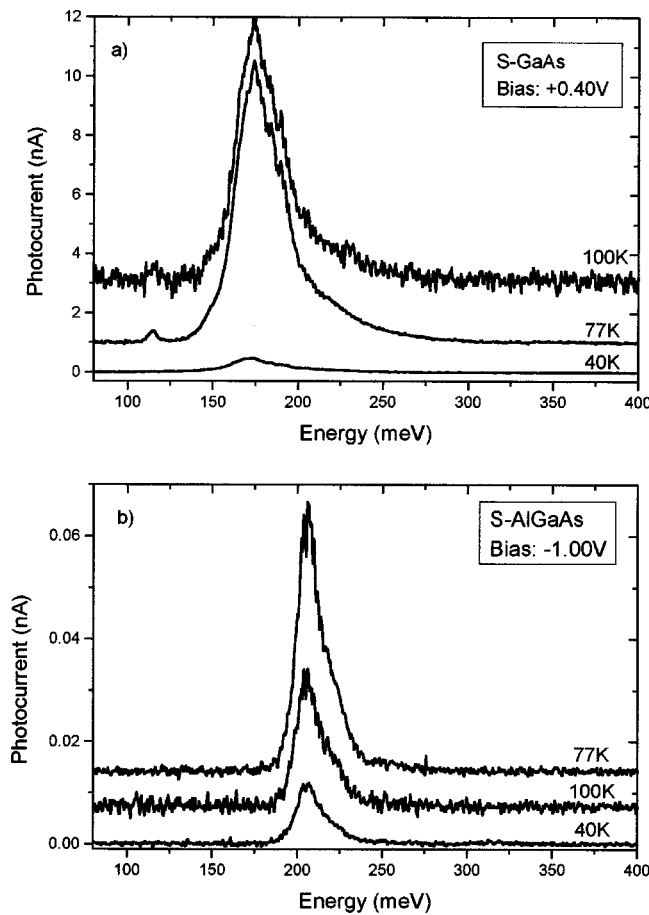


FIG. 7. Intra-band photocurrent spectra of S-GaAs (a) and S-AlGaAs (b) at 40, 77, and 100 K. The equivalent monochromatic optical excitation power is $\sim 10^{-7}$ W.

at different temperatures is, by and large, identical for both QDIPs. The S-AlGaAs has a main intra-band photoresponse peak at 205 meV ($6.0 \mu\text{m}$) with a FWHM of 16 meV ($0.5 \mu\text{m}$), while S-GaAs has a main intra-band photoresponse peak at 175 meV ($7.2 \mu\text{m}$) with a FWHM of 32 meV ($1.3 \mu\text{m}$). Also, S-GaAs shows a small intra-band peak at 115 meV ($10.8 \mu\text{m}$). The addition of the AlGaAs layers leads to a blueshift in the wavelength of peak intra-band photoresponse. The blueshift in intra-band photocurrent peaks, the inter-band photocurrent peaks, and the PLE peaks is attributed to an enhanced confinement potential caused by the inserted AlGaAs layers (as confining layer) as well as to the above-mentioned slight reduction in QD size. A systematic PL/PLE study on single layer PIG InAs/GaAs QD samples suggests that 300 ± 50 meV is the localization energy of the QD electron ground state.¹³ Thus, we attribute the above-mentioned intra-band transitions at 115 and 175 meV to bound-to-bound transitions. Figure 8 shows the intra-band peak intensity as a function of temperature for S-GaAs and S-AlGaAs. Both QDIPs show similar temperature dependence behavior. With increasing temperature, the peak intra-band photocurrent remains unchanged below ~ 40 K, then increases up to ~ 77 K. We explain this as due to the increase in the average electron population in QDs with increasing temperature. Above ~ 77 K, the peak photocurrent begins to

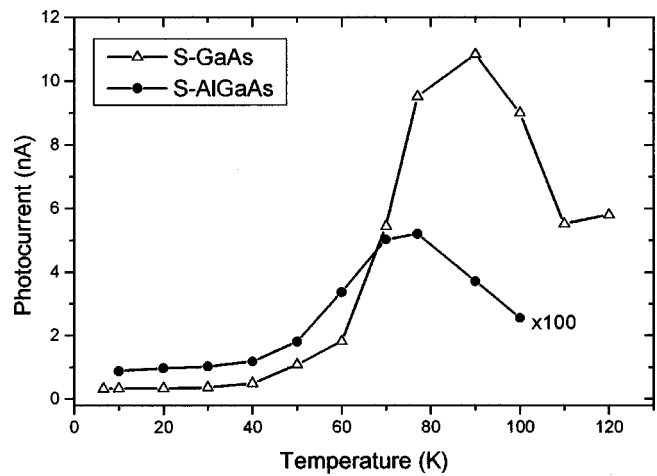


FIG. 8. Intra-band peak photocurrent vs temperature for S-GaAs and S-AlGaAs at a bias of +0.40 and -1.00 V, respectively. The equivalent monochromatic optical excitation power is $\sim 10^{-7}$ W.

decrease. Both QDIPs show maximum intra-band photoreponse at ~ 77 K.

Figures 9(a) and 9(b) show 77 K FTIR intra-band photocurrent spectra of S-GaAs and S-AlGaAs at different bias. The peak positions of the photocurrent spectra at different bias are nearly unchanged for both QDIPs. Figure 10 shows intra-band peak photoresponse as a function of bias for

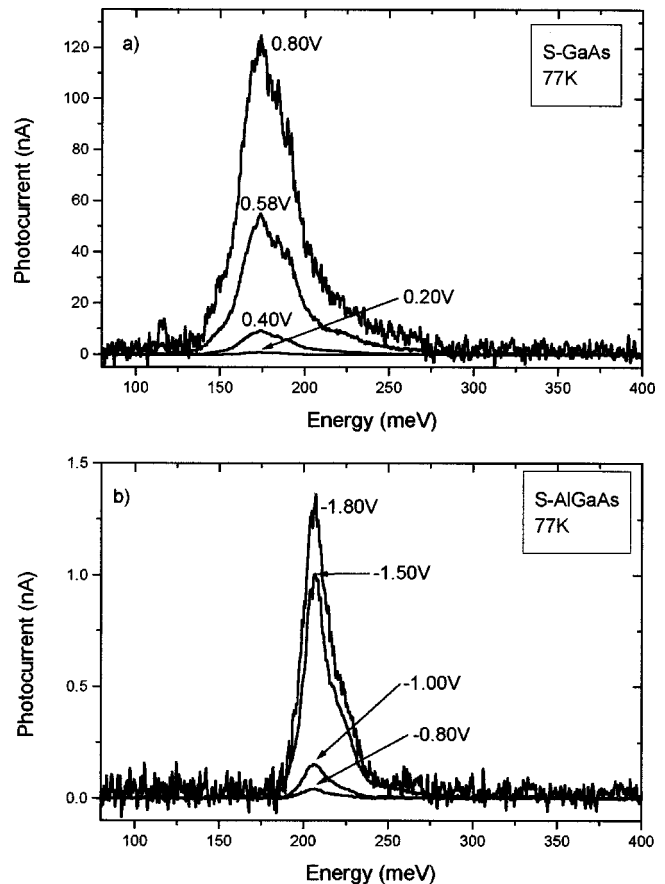


FIG. 9. The 77 K intra-band photocurrent spectra of S-GaAs (a) and S-AlGaAs (b) at different bias. The equivalent monochromatic optical excitation power is $\sim 10^{-7}$ W.

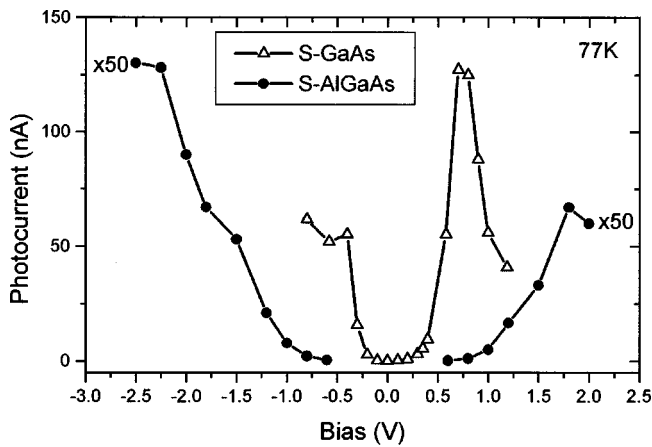


FIG. 10. Bias dependent intra-band peak photoresponse of S-GaAs (a) and S-AlGaAs (b) at 77 K. The equivalent monochromatic optical excitation power is $\sim 10^{-7}$ W.

S-GaAs and S-AlGaAs at 77 K. Both show similar bias-dependent behavior. With increasing bias, the intra-band photoresponse increases slowly at lower bias. Beyond a certain bias (~ 0.4 V for S-GaAs and ~ 1.0 V for S-AlGaAs), it increases rapidly. Namely, both structures show a threshold behavior. The lower threshold bias for S-GaAs compared S-AlGaAs is due to the higher average electron population in QDs of S-GaAs than for S-AlGaAs. With further increase in bias, the photoresponse begins to drop, especially in S-GaAs. This is a negative differential photocurrent phenomenon. Note that the intra-band photocurrent of S-AlGaAs is much weaker than that of S-GaAs due to the additional AlGaAs layers. For S-GaAs, the intra-band photoresponse at zero bias is small but not zero. The existence of this photovoltaic effect implies the presence of a permanent dipole between QD electronic states which originates from the intrinsically asymmetrical potential.¹⁵ In addition, both samples show asymmetric bias dependence between positive and negative bias. Presumably, this is also largely due to the intrinsically asymmetric QD potential.

Figure 11 shows the bias dependence of the dark current of S-GaAs and S-AlGaAs at 77 K. The dark current density of S-AlGaAs is dramatically decreased, up to 10^6 times

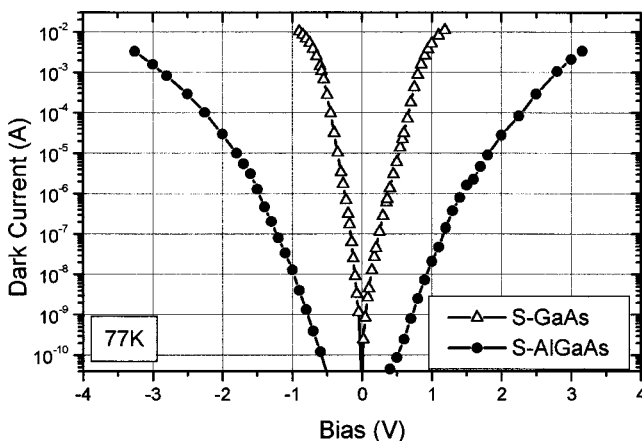


FIG. 11. Dark current of S-GaAs and S-AlGaAs at 77 K.

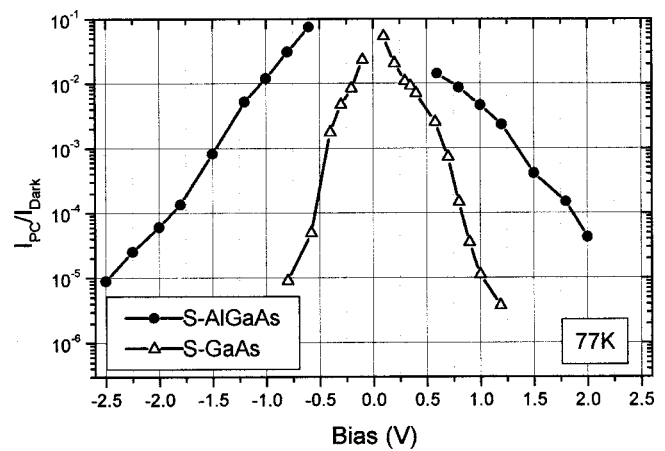


FIG. 12. Photocurrent to dark current ratio (I_{PC}/I_{Dark}) of S-GaAs and S-AlGaAs at 77 K. The equivalent monochromatic optical excitation power is $\sim 10^{-7}$ W.

(from 1 A/cm^2 to 10^{-6} A/cm^2), as compared to that of S-GaAs. This clearly indicates that the AlGaAs barriers added to the QDIP active region act as blocking layers¹⁶ for the dark current (in addition to behaving as confinement layers when placed suitably close to the QDs, as in the samples discussed in this article). The impact of the AlGaAs layer on the photocurrent to dark current ratio is shown in Fig. 12. Within the measured bias range for each sample, the photocurrent to dark current ratio decreases nearly exponentially with increasing bias. The insertion of AlGaAs blocking layers in the QDIP leads to an improvement of up to 10^3 times. This is due to the facts that the reduction of photocurrent by the AlGaAs blocking layer is smaller than that of dark current, and that the QD area is only about 20% of the wetting layer area. Initial measurements on S-GaAs show, at 77 K, an intra-band peak responsivity of $\sim 1 \text{ A/W}$ and peak detectivity larger than $10^9 \text{ cmHz}^{1/2}/\text{W}$ for a bias range of ± 0.2 to ± 0.5 V. This result indicates that QDIPs with undoped active region are feasible. In addition, initial noise tests indicate that this S-GaAs at 77 K is not a background-limited IR photodetector.

SUMMARY

In summary, we have systematically studied structural, optical, electrical, and optoelectronic characteristics of InAs/GaAs as well as InAs/GaAs/AlGaAs/GaAs quantum dot infrared photodetectors with undoped active regions consisting of a unique class of QDs grown via the punctuated island growth (PIG) approach. The InAs QD size, density, as well as QDIP structure and defect density were characterized using AFM and X-TEM. The inter-band transitions of the PIG InAs QDs embedded in n - i - n QDIP structures have been comprehensively characterized with PL, PLE and inter-band photocurrent spectroscopy. Our FTIR based intra- and inter-band photocurrent results show that appropriately designed InAs/AlGaAs QDIPs can serve as a sensor simultaneously for near IR ($\sim 1 \mu\text{m}$) and middle IR radiation. An AlGaAs layer inserted in the active region of QDIPs can serve as a confining layer as well as a blocking layer. The intra-band photoresponse peaks at 115 meV ($10.8 \mu\text{m}$) and 175 meV

(7.2 μm) correspond to bound-to-bound transitions. A line-width of the QDIP intra-band photoresponse as narrow as 16 meV (0.5 μm) has been achieved. These QDIPs with undoped active region show a maximum intra-band photoresponse at ~ 77 K. The initial intra-band responsivity and detectivity results on the QDIPs at 77 K show attractive potential for infrared sensor applications.

ACKNOWLEDGMENTS

This work was supported by AFOSR under the MURI98 program on Nanoscience.

¹U. Bockelmann and G. Bastard, *Phys. Rev. B* **42**, 8947 (1990).

²H. Benisty, C. M. Sotomayer-Torrès, and C. Weisbuch, *Phys. Rev. B* **44**, 10945 (1991).

³V. Ryzhii, *Semicond. Sci. Technol.* **11**, 759 (1996); Y. C. Chang *et al.* (to be published).

⁴D. Pan, E. Towe, and S. Kennerly, *Appl. Phys. Lett.* **73**, 1937 (1998); **75**, 2719 (1999); **76**, 3301 (2000).

⁵S. Maimon, E. Finkman, G. Bahir, S. E. Schacham, J. M. Garcia, and P. M. Petroff, *Appl. Phys. Lett.* **73**, 2003 (1998).

⁶S. J. Xu, S. J. Chua, T. Mei, X. C. Wang, X. H. Zhang, G. Karunasiri,

W. J. Fan, C. H. Wang, J. Jiang, S. Wang, and X. G. Xie, *Appl. Phys. Lett.* **73**, 3153 (1998).

⁷Q. D. Zhuang, J. M. Li, H. X. Li, Y. P. Zeng, L. Pan, Y. H. Chen, M. Y. Kong, and L. Y. Lin, *Appl. Phys. Lett.* **73**, 3706 (1998).

⁸S.-W. Lee, K. Hirakawa, and Y. Shimada, *Appl. Phys. Lett.* **75**, 1428 (1999).

⁹L. Chu, A. Zrenner, G. Böhm, and G. Abstreiter, *Appl. Phys. Lett.* **75**, 3599 (1999).

¹⁰J. Phillips, P. Bhattacharya, S. W. Kennerly, D. W. Beekman, and M. Dutta, *IEEE J. Quantum Electron.* **35**, 936 (1999).

¹¹I. Mukhametzhanov, Z. Wei, R. Heitz, and A. Madhukar, *Appl. Phys. Lett.* **75**, 85 (1999).

¹²Q. Xie, P. Chen, A. Kalburge, T. R. Ramachandran, A. Nayfonov, A. Konkar, and A. Madhukar, *J. Cryst. Growth* **150**, 357 (1995).

¹³I. Mukhametzhanov, Z. H. Chen, O. Baklenov, E. T. Kim, and A. Madhukar, *Phys. Status Solidi B* **224**, 697 (2001).

¹⁴R. Heitz, I. Mukhametzhanov, O. Stier, A. Madhukar, and D. Bimberg, *Phys. Rev. Lett.* **83**, 4654 (1999).

¹⁵Following our observation of the permanent dipole moment and its suggested origin in the underlying asymmetry of the confining potential, theoretical confirmation has been provided by S. J. Sun and Y. C. Chang, *Phys. Rev. B* **62**, 13631 (2001).

¹⁶O. Baklenov, Z. H. Chen, E. T. Kim, I. Mukhametzhanov, A. Madhukar, F. Ma, Z. Ye, B. Yang, and J. Campbell, the 58th IEEE Device Research Conference, Denver, Colorado, June 19–21, 2000, p. 171.